Available online at www.sciencedirect.com
ScienceDirect
Trans. Nonferrous Met. Soc. China 27(2017) 125−133
Transactions of Nonferrous Metals Society of China
www.tnmsc.cn

Structure and properties of micro-arc calcium phosphate coatings on pure titanium and Ti−40Nb alloy

Yurii SHARKEEV[1], Ekaterina KOMAROVA[1], Maria SEDELNIKOVA[1], Ze-ming SUN[2], Qi-fang ZHU[2], Jing ZHANG[2], Tatiana TOLKACHEVA[1], Pavel UVARKIN[1]

1. Institute of Strength Physics and Materials Science of Siberian Branch of Russian Academy of Sciences, 2/4 Academicheskii pr., Tomsk 634055, Russia;
2. Beijing General Research Institute for Non-ferrous Metals, Beijing 100088, China

Received 19 January 2016; accepted 26 August 2016

Abstract: The microstructure, physical and mechanical, and chemical properties of micro-arc calcium phosphate (CaP) coatings deposited under different process voltages in the range of 150−400 V on the commercially pure titanium (Ti) and Ti−40%Nb (Ti−40Nb) (mass fraction) alloy were investigated by the SEM, TEM, XRD and EDX methods. The coating thickness, roughness, and sizes of structural elements were measured and showed similar linear character depending on the process voltage for the coatings on both substrates. SEM results showed the porous morphology with spherical shape structural elements and rough surface relief of the coatings. XRD and TEM studies exhibited the amorphous structure of the CaP coating. With increasing the process voltage to 300−400 V, the crystalline phases, such as $CaHPO_4$ and β-$Ca_2P_2O_7$, were formed onto the coatings. The annealing leads to the formation of complex poly-phase structure with crystalline phases: $CaTi_4(PO_4)_6$, β-$Ca_2P_2O_7$, TiP_2O_7, $TiNb(PO_4)_3$, TiO_2, NbO_2, and Nb_2O_5. The applied voltage and process duration in the ranges of 200−250 V and 5−10 min, respectively, revealed the coating formed on Ti and Ti−40Nb with optimal properties: thickness of 40−70 μm, porosity of 20%−25%, roughness (R_a) of 2.5−5.0 μm, adhesion strength of 15−30 MPa, and Ca/P mole ratio of 0.5−0.7.

Key words: calcium phosphate coating; micro-arc oxidation; Ti−40%Nb alloy; commercially pure titanium; microstructure

1 Introduction

At present metal implants are widely used in medicine to bone tissue replace and to correct its damages and defects. Titanium-, cobalt-, and stainless steel-based alloys are most often used as metal implants in traumatology and orthopaedics [1]. Lately, the third-generation low-modular titanium alloys containing niobium, tantalum, zirconium, and molybdenum become more and more widely used since they are characterized by good ductility and high mechanical strength. The main requirements to metal biomaterials are low elastic modulus compared with that of the human bone (less than 30 GPa) and non-toxicity of alloying components. Regarding the increased biomechanical compatibility, alloys of titanium−niobium system are attractive because they can also possess pseudoelasticity effect approaching their properties to those of the bone tissue [2]. YAO et al [3] reported that the phase stability and elastic modulus of the Ti−Nb β-alloy increased monotonically when the niobium content increased from 5% to 40% (mass fraction). Thus, the Ti−40%Nb (Ti−40Nb) (mass fraction) alloy is the most suitable material for the medical implants providing good biomechanical interaction with the bone tissue.

To increase the biological, chemical, and mechanical properties, different modification methods of the implant surface, such as machining, ion implantation, plasma coating deposition, and electrochemical anodizing are used [4]. The micro-arc oxidation (MAO) method, also known as plasma electrolytic oxidation (PEO) or spark anodizing, is a promising method of surface treatment, since it allows one to obtain

Foundation item: Project (III.23.2.5) supported by the Fundamental Research Program of the Siberian Branch of Russian Academy of Sciences; Project (15-03-07659) supported by the Russian Foundation for Basic Research; Project (CR16-22) supported by the China and Russia on the Implementation of Inter-governmental Scientific and Technological Cooperation Projects of the Notice (NSC foreign word [2012] No. 269)

Corresponding author: Yurii SHARKEEV; Tel: +7-3822-492850; Fax: +7-3822-492576; E-mail: sharkeev@ispms.tsc.ru

DOI: 10.1016/S1003-6326(17)60014-1

biologically active coatings with porous structure. The main advantage of this method is the possibility to control Ca and P ions deposition on the substrate surface due to changing of the electrolyte solution and concentration. Moreover, the MAO method is well suited for the modification and functionalization of the complex shape metal substrates, providing an efficient chemical barrier that prevents escaping of metallic substrate ions and increases the corrosion resistance of titanium alloys [5−7].

It is assumed that after implant introduction into the human organism, transition from the primary mechanical stability caused by the material and design of the implant (primary stability) to the biological stability caused by the surface relief and chemical and hydrophilic properties occurs in the bone tissue–implant joint, which provides the formation of a new bone tissue in the process of osseointegration (secondary stability). Thus, the mechanical strength, structure, morphology, surface implant relief, and chemical properties are important factors in the process of osseointegration which influence the force of contact in the bone tissue–implant interface and can also reduce terms of healing after implant introduction into the human organism [8−10].

The present work is aimed at comparative investigation of the microstructure and physical and mechanical, and chemical properties of the calcium phosphate (CaP) coatings deposited on pure titanium and Ti−40Nb alloy by the MAO method.

2 Experimental

Sample plates (10 mm × 10 mm × 1 mm) were fabricated from commercially pure titanium (Ti, grade 2) and Ti−40Nb alloy. The Ti−40Nb alloy was produced in General Research Institute for Non-ferrous Metals, Beijing, China [11]. The samples were successively ground using SiC abrasive paper with 180, 600, and 1200 grits to remove the natural surface oxide. Then, samples were ultrasonically cleaned sequentially in distilled water and ethanol for 10 min and dried in the air. FEGOSTAEVA et al [12] reported that to carry out micro-arc oxidation for deposition of CaP coatings on specimens, the Micro-arc-3.0 technique was used. The calcium phosphate coatings were deposited from an aqueous solution prepared from 20% phosphoric acid (H_3PO_4) (mass fraction), 6% biological hydroxyapatite (HA, $Ca_{10}(PO_4)_6OH_2$) (mass fraction), and 9% carbonate calcium ($CaCO_3$) (mass fraction) in the anode regime [13]. Micro-arc oxidation process was performed with initial current densities in the range of 0.2−1.0 A/cm^2 using a regulated pulse power supply unit. In the previous works [12−14], we found the optimal micro-arc oxidation parameters for deposition of the CaP coatings on the titanium as follows: pulse frequency of 50 Hz, pulse duration of 100 μs, process duration in the range of 5−10 min, and electrical voltage in the range of 150−400 V. In this work, we used the same MAO parameters for the coating synthesis on the Ti−40Nb alloy substrate. It is known that ordinarily, the MAO method allows to form amorphous coatings with good bioresorption [4−7,9,10,14]. To obtain the crystalline structure of the CaP coatings, some specimens after MAO treatment were subjected to the crystallization annealing at 800 °C for 1 h and the subsequent cooling in the air.

The surface morphology and the structure of the CaP coatings were investigated by scanning electron microscopy (SEM, JEOL JSM−7001F and LEO EVO 50, Zeiss) and transmission electron microscopy (TEM, JEOL JEM−2010). In addition, the elemental compositions and distributions of the coatings were also analyzed using energy-dispersive X-ray spectroscopy (EDX, Pegasus XM2 and INCA, Oxford Instruments) in combination with the SEM systems. The EDX microanalysis was performed in CaP coating micro-areas of top and cross-sectional SEM images. The porosity of the CaP coatings was measured using SEM images. To measure the size of the coating structural elements, the secant method was applied according to the ASTM E1382−9 and DD ENV 1071−5. The porosity (P) was calculated from the formula: $P=\sum l/\sum L\times 100\%$, where L is the length of a secant randomly put on the SEM images and l is the length of the secant part which falls on pores. The number of secants was 50 for each specimen.

For TEM analysis, two types of CaP coating replica were prepared: the first one, indirect method of analysis due to replica removed from CaP layer; the second one, preparation of the cross-section CaP films including cutting slices, polishing slices, and ion milling. Firstly, slices with 2 mm in width and 10 mm in length were cut from the appropriate samples using a diamond wire saw on a slicer (Buehler Isomet low speed saw). Then, stacks were formed by bonding together two slices of the substrate with CaP coating and the substrate was cleaned so that the CaP coating was in the middle. For gluing, Gatan two-component epoxy glue was used. At 100 °C, the hardening time was about 5 min. After annealing, the stack was cut into slices with 1 mm in width on the slicer. Secondly, polishing the slices from each side down to a thickness of about 500 μm was carried out by hand on wet grinding paper. Then, appropriate slices were glued on the metal ring with an outer diameter of 3 mm and an inner diameter of 1.5 mm. After this, appropriate films were polished down to a thickness of about 100 μm. Thirdly, a Gatan 691 precision ion polishing system (PIPS) was used for the ion milling.

The samples were dimpled from both sides by Ar ion beam with a voltage of 5 kV at an angle of 8° for 3 h and at an angle of 6° for 2 h.

The phase composition was determined by X-ray diffractometry (XRD, Bruker D8 Advance) in the angular range of 2θ=10°−90° with a scan step of 0.01° using Cu K_α radiation (λ=0.15405 nm). The surface roughness was estimated with a Hommel−Etamic T1000 profilometer. The traverse length and rate of the measured profile were 6 mm and 0.5 mm/s, respectively. The parameters to be estimated included maximum roughness (R_{max}), average roughness (R_a), and average maximum roughness (R_z) [15]. To measure the CaP coating adhesion strength to the substrate, two cylinders were glued by Loctite Hysol 9514 glue to both sides of the sample with coating. They were fixed in grips in order to be tested under tension in an Instron 1185 machine. The adhesion strength (δ_A) is the maximum stress required to tear the cylinder off the CaP coating. It was measured as $\delta_A=F/S$, where F is the breakout force and S is the separation area [16].

3 Results and discussion

The investigation of the CaP coatings morphology shows that the coatings formed by layers. The structure of the CaP coatings consists of thin porous oxide intermediate sublayer and the basic porous CaP layer. The main components of structure are spheroidal structural elements (spheres) with pores. Figures 1 and 2 show SEM images of the top and cross-sectional CaP coatings on Ti and Ti−40Nb, respectively, deposited under different MAO process voltages. The size of the structural elements depends substantially on the MAO parameters, in particular, on the applied voltage. It was established that the initial process voltage was 150 V. At this voltage, the porous oxide layer is formed and the CaP layer starts to be formed. In this case, the average pore size of coatings on both substrates is 0.5−1.5 μm (Fig. 3), and the total porosity does not exceed 15%.

An increase of the process voltage in the range of 200–300 V leads to the increase of current density and the formation of the porous calcium phosphate layer with spheres and pores. The thickness, roughness, and size of the structural elements and the porosity of coatings grow with increasing the MAO process voltage (Fig. 3, Fig. 4 and Table 1). For the CaP coatings on Ti, the pore and sphere sizes increase to 8 and 25 μm (Fig. 3), consequently; and the total porosity increases to 30%. For the CaP coatings on the Ti–40Nb, the sizes of pores and spheres also increase to 10 and 30 μm (Fig. 3), respectively; moreover, the total porosity increases to 25%. The thickness of the CaP coatings on both substrates grows linearly from 35 to 90 μm with increasing the process voltage (Fig. 4).

The subsequent increase in the process voltage to

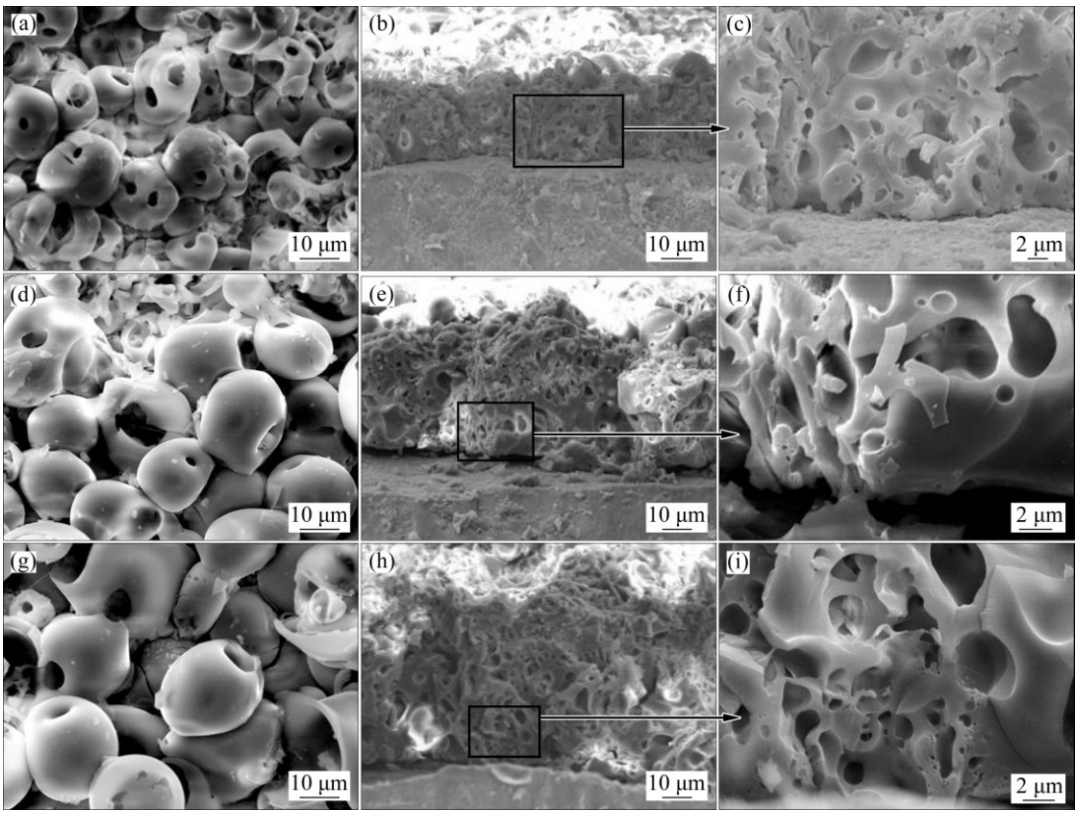

Fig. 1 SEM images of top (a, d, g) and cross-sectional (b, c, e, f, h, i) CaP coatings on Ti deposited under different process voltages: (a−c) 200 V; (d−f) 250 V; (g−i) 300 V

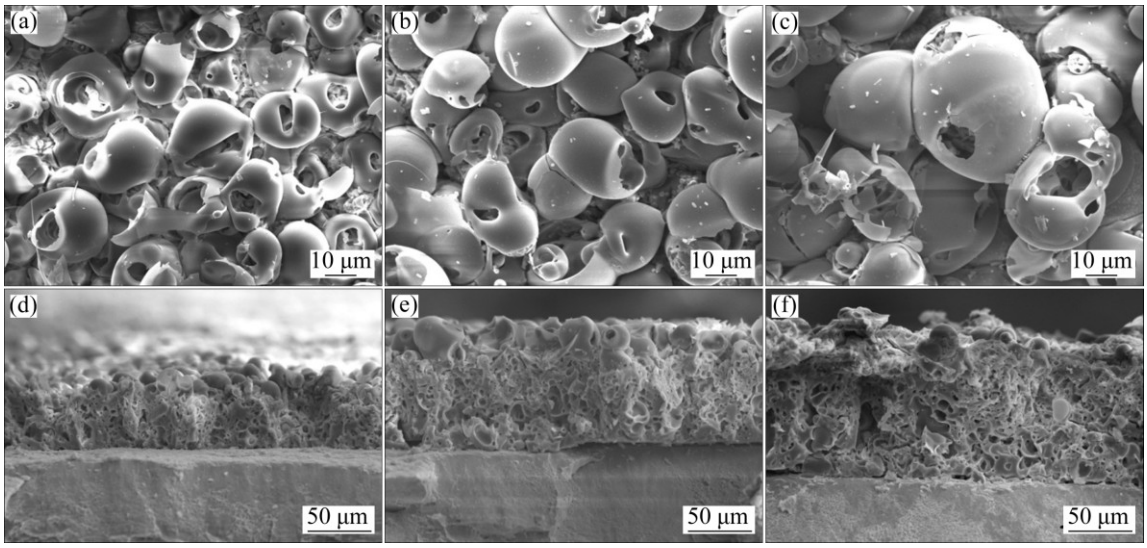

Fig. 2 SEM images of top (a−c) and cross-sectional (d−f) CaP coatings on Ti−40Nb deposited at different process voltages: (a, d) 200 V; (b, e) 250 V; (c, f) 300 V

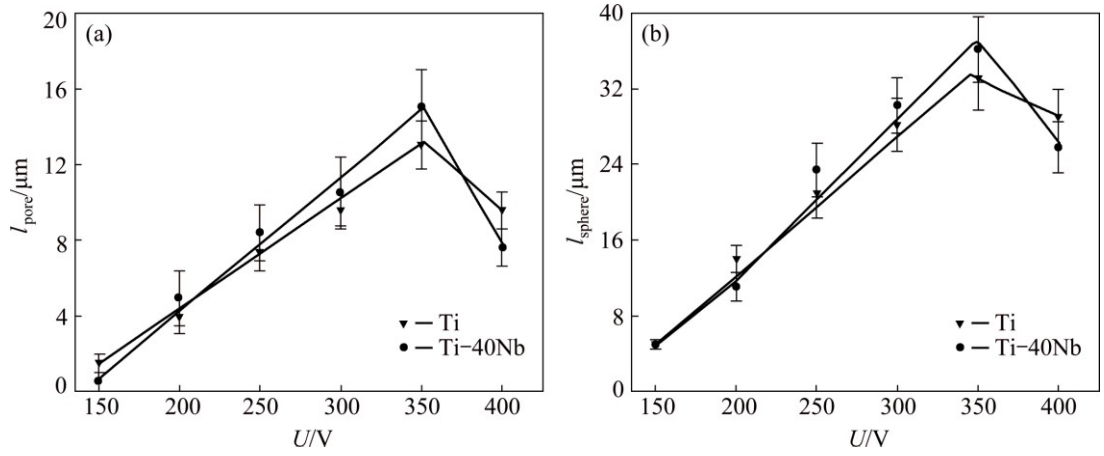

Fig. 3 Plots of pore (a) and sphere (b) sizes against process voltage for CaP coatings on Ti and Ti−40Nb

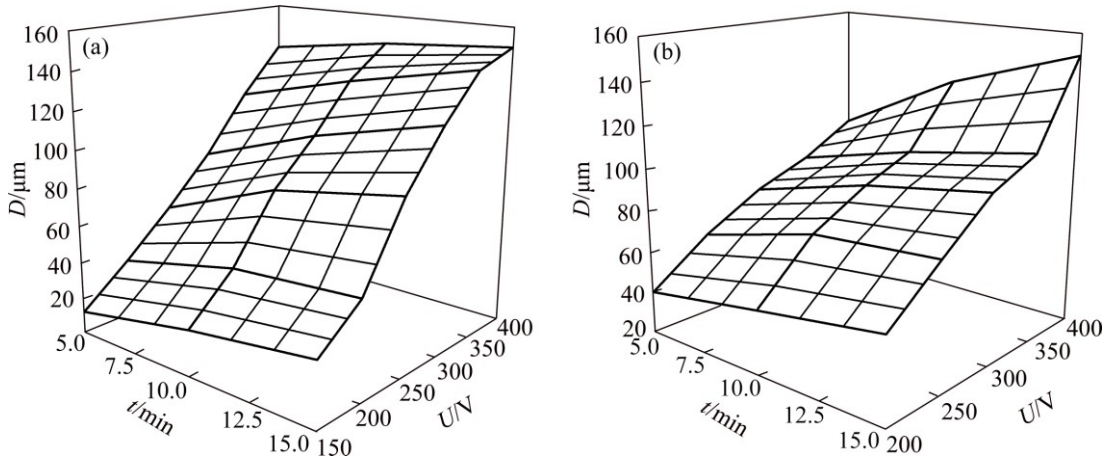

Fig. 4 3D plots of thickness against process voltage and duration for CaP coatings on Ti (a) and Ti−40Nb (b)

400 V is attended with the transformation of the micro-arc discharges in arc ones, thereby causing the sphere destruction and fragmentation and, as a consequence, a decrease in the coating porosity to 15%.

The investigation of the surface roughness shows that the micro-arc CaP coatings on Ti and Ti−40Nb have a rough relief. With increasing the process voltage in the range of 150−400 V and the process duration in the range

of 5−15 min, a linear increase in the roughness parameters R_a, R_z, and R_{max} to 8, 40 and 50 μm, respectively, was observed for the coatings on both substrates (Table 1). In this case, the thickness of the CaP coatings also increases linearly from 20 to 150 μm. KHLUSOV et al [17] reported novel concepts of "niche-relief" and "niche-voltage" for stem cells and supposed that the average roughness in the range of 2.5−5.0 μm was optimal for successful stem cell adhesion onto the coating surface and their further differentiation into the bone tissue. However, COHEN et al [18], PUCKETT et al [19] and WANG et al [20] reported that the surface of titanium implants with nanoroughness strengthens the adhesion of definite cells, i.e., steoblasts (bone-forming cells) and other cellular functions (for example, synthesis of alkaline phosphatase and precipitation of calcium and collagen secretion) and simultaneously suppresses the growth of the competing cells, i.e., fibroblasts (cells creating fibrous tissue and preventing normal bone integration). It should be noted that the surface roughness in the interval of $10\ nm < R_a < 10\ \mu m$ affects the interaction of the biological implants with the bone tissue because it has the same order of magnitude as cells and large biomolecules. At the same time, VERONESI et al [21] and SAMMONS et al [22] reported that microporous rough surfaces improved osseointegration of the implants.

It should be noted that the behavior of the CaP coating formation on the Ti–40Nb alloy and pure titanium is similar in many respects. This was manifested through identical dependences of the sizes of structural elements of spheres and pores (Fig. 3), and the coating thickness (Fig. 4) and surface roughness (Table 1) on the process voltage.

The TEM and XRD analyses demonstrated that the CaP coatings on the Ti and Ti–40Nb are in the X-ray amorphous state, as indicted by two diffusion halos on the selected area diffraction (SAD) patterns (Fig. 5) and by the well pronounced halo on the XRD patterns (Fig. 6). Figure 5 shows the bright-field TEM images with SAD patterns of the CaP coating particles from both substrates. The interpretation of the XRD spectra for the CaP coatings on both substrates deposited under oxidation voltage of 200 V demonstrates the presence of intensive peaks of Ti and Nb, and small reflexes of TiO_2 and NbO_2 (Fig. 6). Existence on XRD patterns of Ti and Nb reflexes may be due to a small thickness of the CaP coatings equal to 15−50 μm (Fig. 4). Poor reflexes of TiO_2 and NbO_2 phases correspond to the oxide intermediate sublayer between the substrate and CaP layer. In this case, the presence of NbO_2 phase is

Table 1 Roughness parameters of micro-arc CaP coatings on Ti and Ti−40Nb

U/V	R_a/μm		R_z/μm		R_{max}/μm	
	Ti	Ti–40Nb	Ti	Ti–40Nb	Ti	Ti–40Nb
150	1.40±0.33	1.32±0.56	9.71±1.74	8.82±0.63	12.71±0.79	10.36±0.52
200	2.78±0.21	3.03±0.17	16.99±0.92	20.09±0.37	18.74±0.98	22.39±0.88
250	4.12±0.13	4.43±0.27	25.66±0.66	28.39±1.82	28.56±0.82	34.02±2.61
300	5.24±0.19	5.48±0.34	31.62±1.12	32.86±1.22	36.79±0.76	38.93±1.45
350	6.05±0.15	6.42±0.30	35.77±0.88	38.73±1.80	39.54±1.14	46.70±2.19
400	7.34±0.25	7.22±0.39	41.74±1.97	39.33±1.96	50.29±3.06	49.51±2.06

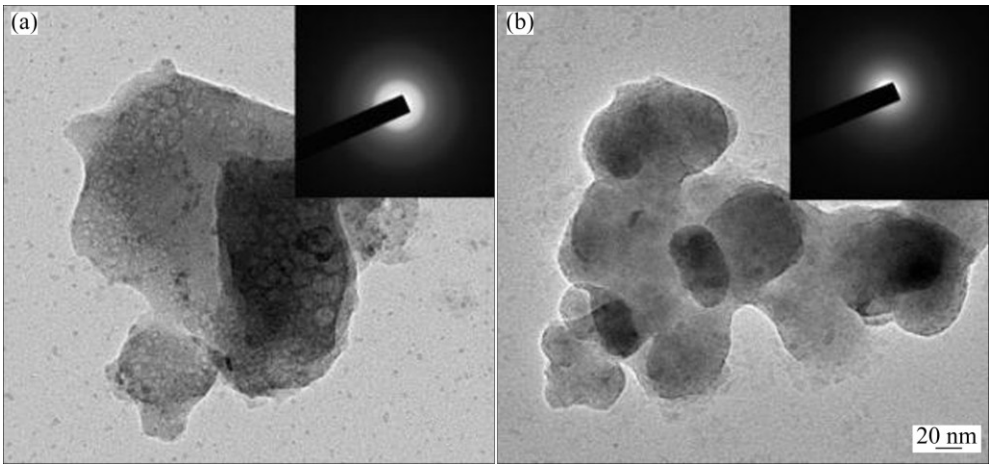

Fig. 5 TEM images with SAD patterns for CaP coating particles removed from Ti (a) and Ti−40Nb (b)

observed in the coatings on Ti−40Nb independent of process voltage, whereas the TiO_2 phase is observed only in the coatings on Ti deposited under low voltages of 150−200 V. We assume that it is connected with electrophysical, thermal, and thermodynamic differences between Ti and Nb as well as their oxides (TiO_2, NbO_2). Nb has a higher thermal conductivity (54.5 W/(m·K)) at 300 K and lower electrical resistivity (0.15 μΩ·m) than Ti (thermal conductivity is 15.5 W/(m·K), and electrical resistivity is 0.55 μΩ·m). Therefore, the MAO process occurs more intensively with the Nb participation, which explains the presence of the niobium oxide and absence of titanium oxide in the phase composition of coatings on Ti−40Nb alloy.

The increase of the process voltage to 300 V leads to the formation in addition to amorphous phase of the crystalline phases such as monetite $CaHPO_4$, and calcium pyrophosphate β-$Ca_2P_2O_7$ in the CaP coatings on both substrates (Fig. 6). The formation of crystalline phases in the coatings is connected with the growth of microplasma discharge temperature above 2000 K. In this case, the poor reflexes of titanium pyrophosphate TiP_2O_7 are observed in XRD patterns of the CaP coatings deposited under 300−400 V just on Ti substrate (Fig. 6(a)). Such compound can be produced as a result of reaction of titanium substrate with phosphoric acid at high temperatures. In this case, the complex Ti- and Nb-incorporated phosphate compound ($TiNb(PO_4)_3$) in amorphous state is formed on Ti−40Nb alloy.

Further increase of the process voltage to 400 V leads to the intensity decrease of the reflexes corresponding to the recognized crystalline phases (Fig. 6). We suppose that it is because the voltage increase leads to the temperature increase in the region of micro-arc discharges above the critical level (>2000 K); therefore, the calcium phosphate layer is destructed. The presence of $CaHPO_4$ and β-$Ca_2P_2O_7$ phases caused the osseoconductive properties of the coatings, which was also confirmed by the biological tests in the previous studies [23,24].

As described above, parts of the specimens were subjected to the crystallization annealing at 800 °C for 1 h and the subsequent cooling in the free regime. The results of the TEM cross-sections (Fig. 7) and XRD analysis (Fig. 8) for such specimens showed that a crystal structure with the complex poly-phase composition was formed in the CaP coatings during annealing. The interpretation of the SAD pattern for the CaP coatings on the Ti represented a set of reflections

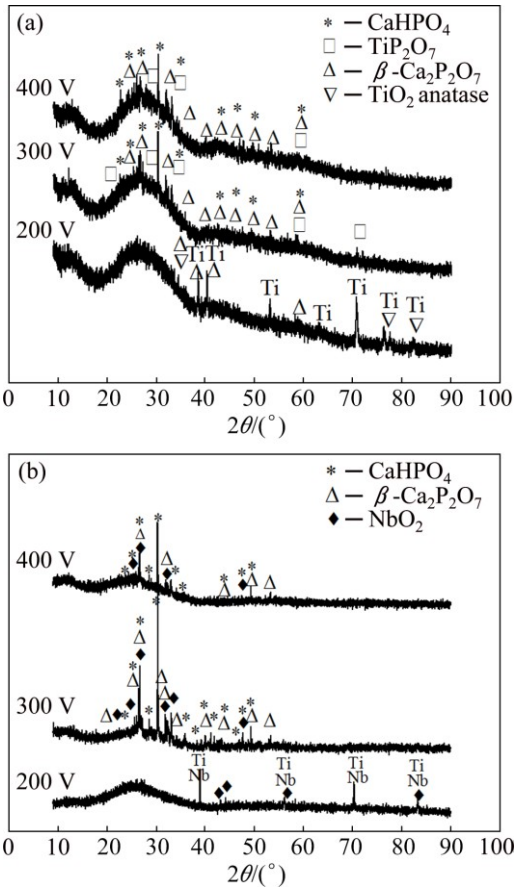

Fig. 6 XRD patterns of micro-arc CaP coatings deposited under different process voltages on Ti (a) and Ti−40Nb (b)

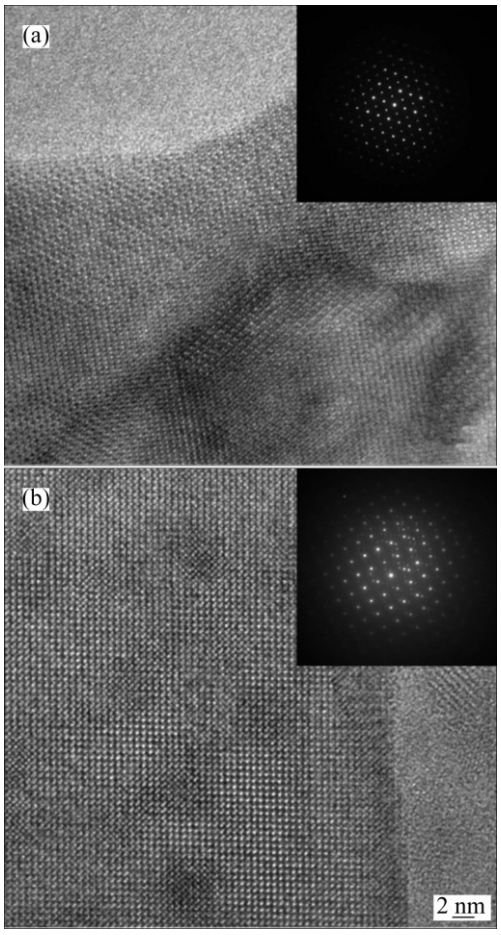

Fig. 7 TEM images with SAD patterns for cross-sectional CaP coatings after annealing on Ti (a) and Ti−40Nb (b)

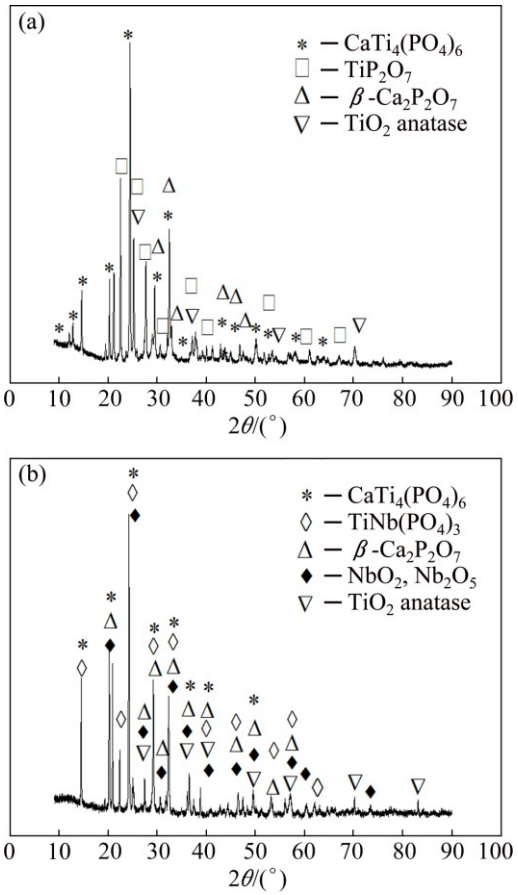

Fig. 8 XRD patterns of CaP coatings after annealing on Ti (a) and Ti−40Nb (b)

corresponding to several phases: the basic phase (double titanium−calcium phosphate $CaTi_4(PO_4)_6$), calcium pyrophosphate β-$Ca_2P_2O_7$, titanium pyrophosphate TiP_2O_7, and titanium dioxide TiO_2 (anatase) (Fig. 7(a)). An analysis of XRD pattern of such coatings confirms the presence of the above-indicated phases (Fig. 8(a)). The interpretation of the SAD patterns (Fig. 7(b)) and XRD pattern (Fig. 8(b)) for the CaP coatings after annealing on the Ti−40Nb illustrates the complex poly-phase composition with the following crystalline phases: the basic phases of double titanium−calcium phosphate $CaTi_4(PO_4)_6$ and titanium−niobium phosphate $TiNb(PO_4)_3$, calcium pyrophosphate β-$Ca_2P_2O_7$, titanium oxide TiO_2, niobium oxides NbO_2, and Nb_2O_5 (Fig. 7(b) and Fig. 8(b)). As is seen from the XRD pattern (Fig. 8), the phase compositions of CaP coatings on Ti is similar to that on Ti–40Nb. Nevertheless, the TiP_2O_7 phase is observed in the CaP coatings on Ti, whereas the complex phosphate compound $TiNb(PO_4)_3$ is present in the CaP coatings on Ti−40Nb, which is in agreement with XRD results (Fig. 6) of CaP coatings before annealing.

The EDX analysis performed from surface and cross-sectional profile of CaP coatings on the Ti substrate revealed the elemental composition (mole fraction) with following elements: (5.6%−11.4% Ca), (17.4%−23.1%P) (52.0%−62.2% O), and titanium (12.3%−17.8% Ti) . The elemental composition (mole fraction) from surface and cross-sectional profile of the CaP coatings on the Ti−40Nb was analogous to that of coatings on the Ti with following elements: (5.6%−11.4% Ca), (17.4%−23.1% P), (52.0%−62.2% O), (8.1%−12.1% Ti), and (3.4%−7.9% Nb). The larger amount of Ti than Nb in the coatings is connected with predominant Ti content in amorphous state. It was confirmed by the TEM (Fig. 7(b)) and XRD (Fig. 8(b)) results for CaP coatings after annealing, which showed the crystalline structure with numerous Ti-containing compounds.

With increasing the process voltage to 300 V, the mole ratios of Ca to P (n(Ca)/n(P)) for the coatings increase linearly from 0.3 to 0.7 (for the bone tissue, n(Ca)/n(P)=1.67) (Fig. 9(a)). With the increase of the voltage and, as consequently, the temperature in the microplasma discharge area, the deposition of Ca^{2+} ions from the electrolyte intensifies. In this case, the crystalline phases $CaHPO_4$ and β-$Ca_2P_2O_7$ are formed in the coatings. As a result, the Ca content and the n(Ca)/n(P) increase. Further increase in the process voltage to 400 V leads to the decrease of the n(Ca)/n(P) to 0.45 (Fig. 9(a)). It is connected with the fact that the

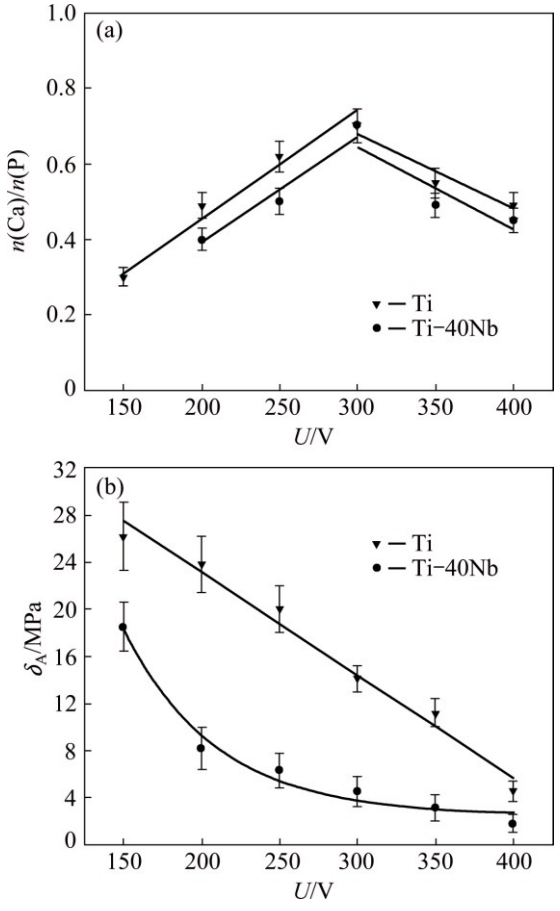

Fig. 9 Plot of n(Ca)/n(P) (a) and adhesion strength δ_A (b) against process voltage for CaP coatings on Ti and Ti−40Nb

voltage increase leads to the temperature increase in the region of micro-arc discharges above the critical level (> 2000 K). Therefore, the CaP coatings are destructed. However, the n(Ca)/n(P) for cross-sectional profile of the coatings on both substrates does not exceed 0.4, which is connected with the presence of large amount of oxide and phosphate compounds near the substrate.

It is well known that the basic characteristic of the coatings is the adhesion strength to the substrate. According to the ISO 13779−4, for medical devices with coatings, the adhesion strength must be not less than 15 MPa. In the present work, it is demonstrated that the adhesion strengths of the micro-arc CaP coatings on Ti and Ti−40Nb decrease with increasing the MAO voltage (Fig. 9(b)). This is due to the increase of the coating thickness and porosity. For the coatings on Ti, it was established that the maximum process voltage at which the coating adhesion to the substrate was not lower than 15 MPa was 300 V. Unfortunately, the adhesion strength of the CaP coatings on the Ti−40Nb was less than 17 MPa (Fig. 9(b)), which was insufficient for their applications. In this regard, to increase the coating adhesion to the substrate, the surface was preliminary treated using sandblasting and subsequent chemical etching of the sample surface before the coating deposition [12,14]. This allows to increase adhesion strength of the coating to the substrate to 30 MPa for the coatings deposited under process voltages of 150−250 V.

It has been revealed that the process voltage of 300 V is critical for the formation of the CaP coatings on both substrates. The increase of the process voltage above this value leads to the decrease of the coating adhesion strength, n(Ca)/n(P) and total porosity to below 15 MPa, 0.45 and 15%, respectively (Fig. 9).

4 Conclusions

1) Comparative investigations of CaP coatings on the pure Ti and Ti−40Nb alloy deposited by the MAO method showed that the behavior of the coating formation on both substrates was similar in many respects. This was manifested through identical dependences of the sizes of structural elements (spheres and pores), and the coating thickness and surface roughness on the process voltage which were linear in character.

2) XRD and TEM analyses showed that the CaP coatings on both substrates were in the X-ray amorphous state after deposition under process voltages of 200−250 V. With increasing the process voltage to 300−400 V, the crystalline phases such as $CaHPO_4$ and β-$Ca_2P_2O_7$ were formed on the coatings. After annealing the crystalline, poly-phase structure was formed in the coatings with the following phases: $CaTi_4(PO_4)_6$, β-$Ca_2P_2O_7$, TiP_2O_7, $TiNb(PO_4)_3$, TiO_2, NbO_2 and Nb_2O_5.

3) The MAO applied voltage and process duration in the ranges of 200−250 V and 5−10 min, respectively, provide the formation of the micro-arc CaP coatings on the pure Ti and Ti−40Nb alloy with the maximum n(Ca)/n(P) of 0.5−0.7, maximum adhesion strength of 20−25 MPa, coating thickness of 40−70 μm, porosity of 20%−25% and average roughness of 2.5−5.0 μm.

Acknowledgements

The authors are grateful to Dr. E. V. LEGOSTAEVA and main specialist A. I. TOLMACHEV from Institute of Strength Physics and Materials Science SB RAS (Tomsk, Russia) for help in performance of some experiments and discussion of results.

References

[1] LUO Yong, GE Shi-rong, JIN Zhong-min. Wettability modification for biosurface of titanium alloy by means of sequential carburization [J]. Journal of Bionic Engineering, 2009, 6: 219−223.

[2] ZHURAVLEVA K, MULLER R, SCHULTZ L, ECKERT J, GEBERT A, BOBETH M, CUNIBERTI G. Determination of the Young's modulus of porous β-type Ti−40Nb by finite element analysis [J]. Materials & Design, 2014, 64: 1−8.

[3] YAO Qiang, SUN Jian, XING Hui, GUO Wen-yuan. Influence of Nb and Mo contents on phase stability and elastic property of β–type Ti−X alloys [J]. Transactions of Nonferrous Metals Society of China, 2007, 17: 1417−1421.

[4] KULKARNI M, MAZARE A, SCHMUKI P, IGLIC A. Biomaterial surface modification of titanium and titanium alloys for medical applications [C]//Nanomedicine. London: One Central Press, 2014: 111−136.

[5] EVCHEVERRY−RENDON M, GALVIS O, GIRALDO D Q, PAVON J, LOPEZ−LACOMBA J L, JIMENEZ−PIQUE E, ANGLADA M, ROBLEDO S M, CASTANO J G, ECHEVERRIA F. Osseointegration improvement by plasma electrolytic oxidation of modified titanium alloys surfaces [J]. Journal of Materials Science (Materials in Medicine), 2015, 26: 71−88.

[6] SHARKEEV Y P, SHEYKIN V V, SEDELNIKOVA M B, LEGOSTAEVA E V, KOMAROVA E G, ERMAKOV V V, OSIPOV A N, SHELEKHOVA E A. Modification of titanium medical agraffe surface for suturing instruments with micro arc oxidation method [J]. Inorganic Materials: Applied Research, 2016, 7: 226−232.

[7] KOYANO K, ATSUTA I, JINNO Y. Anodized surface and its clinical performance [C]//Implant Surfaces and their Biological and Clinical Impact. Heideberg: Springer, 2014: 137−145.

[8] RAGHAVENDRA S, WOOD M C, TAYLOR T D. Early wound healing around endosseous implants: A review of the literature [J]. The International Journal of Oral & Maxillofacial Implants, 2005, 20: 425−431.

[9] TABASSUM A, MEIJER G, WALBOOMERS X F, JANSEN J A. Evaluation of primary and secondary stability of titanium implants using different surgical techniques [J]. Clinical Oral Implants Research, 2014, 25: 487−492.

[10] ANITUA E, PRADO R, ORIVE G, RICARDO T. Effects of calcium-modified titanium implant surfaces on platelet activation, clot formation, and osseointegration [J]. Journal of Biomedical Materials Research, 2015, 103: 969−980.

[11] SHARKEEV Y P, EROSHENKO A Y, GLUCHOV I A, ZHU Q, TOLMACHEV A I. Microstructure and mechanical properties of

Ti40Nb alloy after severe plastic deformation [C]//Proceedings of AIP Conference. Melville, NY: AIP Publishing, 2014: 567−570.
[12] LEGOSTAEVA E V, SHARKEEV Y P, TOLKACHEVA T V, TOLMACHEV A I, UVARKIN P V. Bioactive coating on titanium implant and method for making thereof: WIPO Patent, 02385740 [P]. 2010−04−10.
[13] SHASHKINA G A, SHARKEEV Y P, KOLOBOV Y P, KARLOV A V. Calcium phosphate coating for titanium and its alloys, method for forming such coating: WIPO Patent, 02291918 [P]. 2007−01−20.
[14] SHARKEEV Y P, PSAKHIE S G, LEGOSTAEVA E V, KNYAZEVA A G, SMOLIN A Y, EROSHENKO A Y, KONOVALENKO I S, NAZARENKO N N, BELYAVSKAYA O A, KULYASHOVA K S, KOMAROVA E G, TOLKACHEVA T V, KHLUSOV I A, ZAITSEV K V, KHLUSOVA M Y, POLENICHKIN V K, SERGIENKO V I, GNEDENKOV S V, SINEBRYUKHOV S L, PUZ' A V, KHRISANFOVA O A, EGORKIN V S, ZAVIDNAYA A G, TERLEEVA O P, MIRONOV I V, SLONOVA A I, LYAMINA G V, FORTUNA S V, YAKOVLEV V I, KULAKOV A A, GVETADZE R S, KHAMRAEV T K, ABRAMIAN S V. Biocomposites based on calcium-phosphate coatings, nanostructured and ultrafine-grained bioinert metals, their biocompatibility and biodegradation [M]. Tomsk: Publishing House of Tomsk State University, 2014.
[15] GADELMAWLA E S, KOURA M M, MAKSOUD T M A, ELEWA I M, SOLIMAN H H. Roughness parameters [J]. Journal of Materials Processing Technology, 2002, 123: 133−145.
[16] TUSHINSKIY L I, PLOKHOV A V, TOKAREV A O, SINDEEV V I. Methods for investigations of materials [M]. Moscow: Mir, 2004.
[17] KHLUSOV I A, DEKHTYAR Y, KHLUSOVA M Y, GOSTISCHEV E A, SHARKEEV Y P, PICHUGIN V F, LEGOSTAEVA E V. Novel concepts of "niche-relief" and "niche-voltage" for stem cells as a base and hematopoietic tissues biomimetic engineering [C]// Proceedings of IFMBE. Heidelberg: Springer, 2013: 99−102.
[18] COHEN A, LIU-SYNDER P, STOREY D, WEBSTER T J. Decreased fibroblast and increased osteoblast functions on ionic plasma deposited nanostructured Ti coatings [J]. Nanoscale Research Letters, 2007, 2: 385−390.
[19] PUCKETT S, PARETA R, WEBSTER T J. Nano rough micron patterned titanium for directing osteoblast morphology and adhesion [J]. International Journal of Nanomedicine, 2008, 3: 229−241.
[20] WANG P, ZHAO L, LIU J, WEIR M D, ZHOU, XU H H K. Bone tissue engineering via nanostructured calcium phosphate biomaterials and stem cells [J]. Bone Research, 2014, 2: 1−13.
[21] VERONESI F, GIAVARESI G, GUARINO V, RAUCCI M G, SANDRI M, TANPIERI A, AMBROSIO L, MILENA F. Bioactivity and bone healing properties of biomimetic porous composite scaffold: In vitro and in vivo studies [J]. Journal of Biomedical Materials Research (Part A), 2015, 103: 2932−2941.
[22] SAMMONS R L, LUMBIKANONDA N, GROSS M, CANTZLER P. Comparison of osteoblast spreading on microstructured dental implant surfaces and cell behavior in an explant model of osseointegration: A scanning electron microscopic study [J]. Clinical Oral Implants Research, 2005, 16: 657−666.
[23] SHARKEEV Y P, KOLOBOV Y R, KARLOV A V, KHLUSOV I A, LEGOSTAEVA E V, SHASHKINA G A. Structure, mechanical characteristics and osteogenic properties of a biocomposite on the basis of submicrocrystalline titanium and microarc calcium−phosphate coating [J]. Fizicheskaya Mezomekhanika, 2005, 8: 83−86.
[24] LEGOSTAEVA E V, KHLUSOV I A, SHARKEEV Y P, KARLOV A V, SHASHKINA G A. Evolution of the structure and properties of the biocomposite based on the nanostructured titanium and microarc calcium phosphate coatings at interaction with the biomedium [J]. Fizicheskaya Mezomekhanika, 2006, 9: 205−208.

钛和 Ti−40Nb 合金的微弧磷酸钙涂层结构与性能

Yurii SHARKEEV[1], Ekaterina KOMAROVA[1], Maria SEDELNIKOVA[1],
Ze-ming SUN[2], Qi-fang ZHU[2], Jing ZHANG[2], Tatiana TOLKACHEVA[1], Pavel UVARKIN[1]

1. Institute of Strength Physics and Materials Science of Siberian Branch of Russian Academy of Sciences, 2/4 Academicheskii pr., Tomsk 634055, Russia;
2. 北京有色金属研究总院，北京 100088

摘　要：采用 SEM、TEM、XRD 和 EDX 等试验手段对经 150~400 V 电压微弧氧化处理后工业纯钛(Ti)和 Ti−40%Nb(Ti−40Nb)(质量分数)合金表面磷酸钙(CaP)涂层的显微组织、物理和力学性能以及化学特性进行研究。结果表明：在两种基体上所得到的涂层厚度、粗糙度和结构元尺寸显示出相似的线性特征且与处理电压有关。扫描电镜(SEM)分析表明，磷酸钙涂层为多孔形态，表面呈粗糙浮雕状。XRD 和 TEM 分析结果表明，微弧磷酸钙涂层呈非晶态结构。当氧化电压增加至 300~400 V 时，涂层中形成了结晶相，如 $CaHPO_4$、β-$Ca_2P_2O_7$。经过退火处理，涂层中形成复杂的多相结构，如 $CaTi_4(PO_4)_6$、β-$Ca_2P_2O_7$、TiP_2O_7、$TiNb(PO_4)_3$、TiO_2、NbO_2 和 Nb_2O_5。当氧化电压为 200~250 V、处理时间为 5~10 min 时，在工业纯钛和 Ti−40Nb 合金表面形成的涂层显示出最佳特性，其厚度为 40~70 μm，孔隙率为 20%~25%，粗糙度(R_a)为 2.5~5.0 μm，粘合强度为 15~30 MPa，Ca 与 P 最佳摩尔比为 0.5~0.7。

关键词：磷酸钙涂层；微弧氧化；Ti−40%Nb 合金；工业纯钛；显微组织

(Edited by Wei-ping CHEN)